ChemPubSoc Europe

DOI: 10.1002/celc.202000001

CHEMELECTROCHEM Articles

Co-reactant and Annihilation Electrogenerated Chemiluminescence of $[Ir(df\text{-}ppy)_2(ptb)]^+$ Derivatives

Lachlan C. Soulsby,[a] Johnny Agugiaro,[b] David J. D. Wilson,*[b] David J. Hayne,[c] Egan H. Doeven,[d] Lifen Chen,[a, e] Tien T. Pham,[a] Timothy U. Connell,[a, f] Aaron J. Driscoll,[a] Luke C. Henderson,[c] and Paul S. Francis*[a]

The $[Ir(df\text{-}ppy)_2(ptb)]^+$ complex (where df-ppy = 2-(2,4-difluorophenyl)pyridine anion; ptb = 1-benzyl-1,2,3-triazol-4-ylpyridine) has previously been shown to be a promising blue luminophore for electrogenerated chemiluminescence (ECL). Herein, we examine the ECL of three $[Ir(df\text{-}ppy)_2(ptb)]^+$ derivatives (containing df(CF_3)-ppy-Me, df(CN)-ppy, or df-ppy-CF_3 ligands) in comparison with the parent complex. In the annihilation mode, all four complexes exhibited ECL, although the emission from $[Ir(df(CN)\text{-}ppy)_2(ptb)]^+$ was weak and red-shifted from its photoluminescence. The absence of this shift in the corresponding reductive-oxidation co-reactant ECL with benzoyl peroxide (BPO), and the very low ECL intensity in oxidative–reductive co-reactant ECL with tri-*n*-propylamine (TPrA) enables this effect to be ascribed to oxidative degradation. The $[Ir(df\text{-}ppy\text{-}CF_3)_2(ptb)]^+$ complex gave the greatest ECL intensities of the four $[Ir(C^N)_2(ptb)]^+$ complexes in the annihilation mode and through both co-reactant pathways, and shows great potential as a blue electrochemiluminophore. In "mixed annihilation" ECL experiments involving the oxidation of $Ir(ppy)_3$ and the reduction of the $[Ir(C^N)_2(ptb)]^+$ complexes, only $[Ir(df\text{-}ppy)_2(ptb)]^+$ and $[Ir(df(CF_3)\text{-}ppy\text{-}Me)_2(ptb)]^+$ elicited the green ECL from $Ir(ppy)_3$*, as the electron-withdrawing substituents on the other two complexes lower the SOMO energy of the reduced complexes below that required to attain the $Ir(ppy)_3$* excited state upon reaction with $[Ir(ppy)_3]^+$.

1. Introduction

The evolution of light from a chemical reaction in which at least one reactant has been electrochemically generated is termed 'electrochemiluminescence', 'electrogenerated chemiluminescence' or ECL.[1] There are two general routes for ECL, referred to as annihilation and co-reactant.[2] In the annihilation pathway, the luminophore is both oxidized and reduced (typically by applying a two-step potential pulse sequence). These species then react to form the excited product that is responsible for the emission. Alternatively, the addition of a 'co-reactant' enables the initiation of ECL by applying only an oxidative or reductive potential.[3] In anodic (or 'oxidative-reduction') co-reactant ECL, oxidation of the co-reactant molecule forms a strong reducing agent that reacts with the oxidized luminophore to form the electronically excited product. Anodic co-reactants include tri-*n*-propylamine (TPrA)[4] (Scheme 1) and oxalate ($C_2O_4^{2-}$).[3,5] In cathodic (or 'reductive-oxidation') co-reactant ECL, reduction of the co-reactant molecule forms a strong oxidizing agent that reacts with the reduced luminophore to form the excited product. Cathodic co-reactants include benzoyl peroxide (BPO)[6] (Scheme 2) and peroxydisulfate ($S_2O_8^{2-}$).[7]

Typically, only one luminophore is used, but ECL systems containing multiple metal complex luminophores have been increasingly explored.[1c,9] Under annihilation ECL conditions, this can be exploited for enhanced ECL intensity from the lower

$$TPrA \rightarrow TPrA^{+\bullet} + e^-$$
$$M \rightarrow M^+ + e^-$$
$$TPrA^{+\bullet} \rightarrow TPrA^{\bullet} + H^+$$
$$M^+ + TPrA^{\bullet} \rightarrow M^* + \text{additional products}$$
$$M^* \rightarrow M + h\nu$$

Scheme 1. TPrA co-reactant ECL mechanism in which both the metal complex (M) and co-reactant are electrochemically oxidized.[4a] Alternative pathways, including one in which only the co-reactant is oxidized,[4b] have also been identified. The feasibility of these pathways for any metal complex electrochemiluminophore can be predicted from the reduction potentials and emission energy of the complex.[4c]

[a] L. C. Soulsby, Dr. L. Chen, T. T. Pham, Dr. T. U. Connell, A. J. Driscoll, Prof. P. S. Francis
School of Life and Environmental Sciences
Faculty of Science, Engineering and Built Environment
Deakin University, Geelong, Victoria 3220, Australia
E-mail: paul.francis@deakin.edu.au
[b] J. Agugiaro, Prof. D. J. D. Wilson
Department of Chemistry and Physics
La Trobe Institute for Molecular Science
La Trobe University, Melbourne, Victoria 3086, Australia
E-mail: david.wilson@latrobe.edu.au
[c] Dr. D. J. Hayne, Prof. L. C. Henderson
Institute for Frontier Materials, Deakin University
Geelong, Victoria 3220, Australia
[d] Dr. E. H. Doeven
Centre for Regional and Rural Futures
Faculty of Science, Engineering and Built Environment
Deakin University, Geelong, Victoria 3220, Australia
[e] Dr. L. Chen
Current affiliation:
College of Biological, Chemical Sciences and Engineering
Jiaxing University, Jiaxing 314001, P.R. China
[f] Dr. T. U. Connell
Current affiliation:
RMIT University
Melbourne, Victoria 3001 Australia

Supporting information for this article is available on the WWW under https://doi.org/10.1002/celc.202000001

$$BPO + e^- \rightarrow PhCO_2^{\bullet} + PhCO_2^-$$
$$M + e^- \rightarrow M^-$$
$$M^- + PhCO_2^{\bullet} \rightarrow M^* + PhCO_2^-$$
$$M^* \rightarrow M + h\nu$$

Scheme 2. BPO co-reactant ECL mechanism where M represents a metal complex.[6a,c,d] Alternative pathways have also been described.[6b,8]

energy emitter,[10] a combination of emissions to give a range of colors,[10d,11] or spatially resolved ECL of the same or different spectral distribution at the working and counter electrodes.[12] Co-reactant ECL systems containing multiple metal complex luminophores have also been examined,[13] with focus on developing multi-color (multiplexed) detection systems. The development of multi-luminophore ECL systems is underpinned by the emergence of cyclometalated iridium(III) complexes exhibiting a wide range of emission colors.[9,14] The emission can be tuned through control of the ligand environment to manipulate the frontier molecular orbital energies, with commensurate shifts in the corresponding reduction potentials. Density functional theory (DFT) calculations help to understand the influence of these changes,[15] and could ideally enable the prediction of properties prior to synthesis.[14c]

We have previously examined the annihilation ECL of a mixture of $Ir(ppy)_3$ (a well characterized green luminophore) with $[Ir(df\text{-}ppy)_2(ptb)]^+$ (a blue luminophore).[16] The application of alternating potentials sufficient to reduce $[Ir(df\text{-}ppy)_2(ptb)]^+$ and oxidize $Ir(ppy)_3$ generated ECL from the green luminophore at much greater intensities than those obtained through its conventional annihilation ECL. Moreover, when applying alternating potentials sufficient to reduce $[Ir(df\text{-}ppy)_2(ptb)]^+$ and oxidize both complexes, the emission could occur from both luminophores and the overall ECL spectrum was dependent on their relative concentration. We also prepared $[Ir(df\text{-}ppy\text{-}CF_3)_2(ptb)]^+$ after DFT calculations indicated that the mixed annihilation ECL reaction involving the reduced $[Ir(df\text{-}ppy(CF_3))_2(ptb)]^0$ and the oxidized $[Ir(ppy)_3]^+$ species would not be sufficiently energetic to attain the excited state of either luminophore. The prediction was experimentally verified, and the conventional annihilation ECL of either complex could be exclusively generated in the presence of the other, although the intensity was greatly diminished by parasitic dark reactions.[16]

Herein we present an evaluation of the electrochemical, spectroscopic, annihilation ECL and co-reactant ECL properties of three blue emitting $[Ir(df\text{-}ppy)_2(ptb)]^+$ derivatives. This enabled assessment of the accuracy of DFT-based predictions from our previous work, and provided new insight into the utility of this promising class of blue electrochemiluminophores.

2. Results and Discussion

The $[Ir(df\text{-}ppy)_2(ptb)]^+$ complex and three closely related derivatives (Figure 1) were synthesized from commercially available precursors ($[Ir(C^\wedge N)_2(\mu\text{-}Cl)]_2$ where C^N = df-ppy, df(CF_3)-ppy-Me, df-ppy-CF_3, or df(CN)-ppy). The range of electron

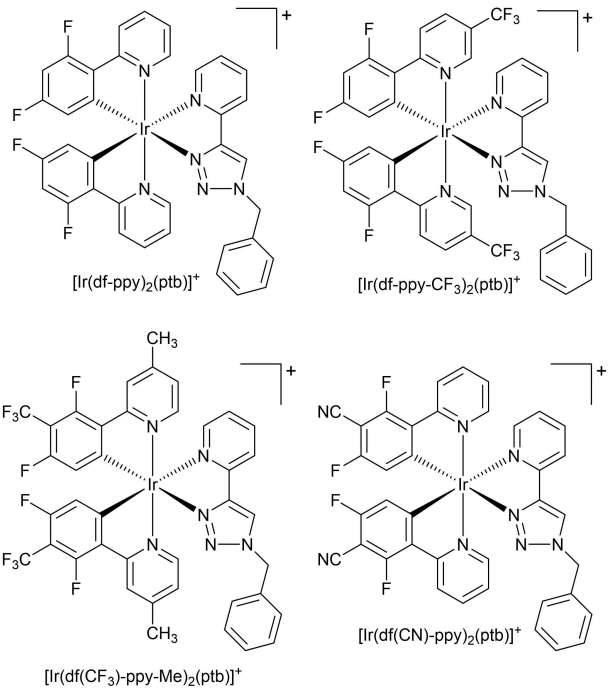

Figure 1. Chemical structures of $[Ir(df\text{-}ppy)_2(ptb)]^+$ and three derivatives examined in this study.

withdrawing/donating substituents on the phenyl and/or pyridyl ring of the df-ppy ligands enabled interrogation of electrogenerated chemiluminescence properties upon subtle changes in ligand structure.

2.1 Spectroscopy

Similar to $[Ir(df\text{-}ppy)_2(ptb)]^+$,[17] the three derivatives exhibit strong absorption bands between 220 nm and 320 nm (Table 1 and Figure S1), attributable to π-π* ligand-centered transitions, with the most intense bands centered at 244–249 nm involving transitions on the df-ppy ligands and the triazole group, and shoulders at 300–320 nm associated with the pyridine groups.[17a] Weaker bands at 320–450 nm correspond to d-π* MLCT transitions. Room temperature and low-temperature (85 K) photoluminescence emission spectra showed resolved vibronic structure (Table 1 and Figure S2), with emission energies increasing in the order: $[Ir(df\text{-}ppy\text{-}CF_3)_2(ptb)]^+ < [Ir(df\text{-}ppy)_2(ptb)]^+ < [Ir(df(CF_3)\text{-}ppy\text{-}Me)_2(ptb)]^+ \approx [Ir(df(CN)\text{-}ppy)_2(ptb)]^+$.

2.2 Electrochemistry

As shown in Table 2, the values of $E^{0\prime}(M^+/M)$, $E^{0\prime}(M/M^-)$ and ΔE determined by cyclic voltammetry for the novel complexes $[Ir(df(CF_3)\text{-}ppy\text{-}Me)_2(ptb)]^+$ and $[Ir(df(CN)\text{-}ppy)_2(ptb)]^+$ were in good agreement (within 0.03 V) with those predicted from the difference in MO energies compared to the $[Ir(df\text{-}ppy)_2(ptb)]^+$ complex.[16] The reduction potentials of the novel complexes fall

Table 1. Spectroscopic properties of $Ir(ppy)_3$ and the four $[Ir(C^{\wedge}N)_2(ptb)]^+$ complexes.

Complex	Absorbance λ_{max}[b] [nm]	Photoluminescence[a] λ_{max}[b] (r.t.) [nm]	λ_{max}[b] (r.t.) [eV]	λ_{max}[c] (85 K) [nm]	λ_{max}[c] (85 K) [eV]
$Ir(ppy)_3$	240, 281, 373	520	2.38	494, 531, 578(sh)	2.51
$[Ir(df\text{-}ppy)_2(ptb)]^+$	245, 302(sh), 359	453, 483	2.74	448, 480, 506, 516	2.77
$[Ir(df(CF_3)\text{-}ppy\text{-}Me)_2(ptb)]^+$	245, 302(sh), 348(sh)	445, 473	2.79	439, 470, 496, 504	2.82
$[Ir(df(CN)\text{-}ppy)_2(ptb)]^+$	244, 277(sh), 329(sh), 359 (sh)	444, 473	2.79	440, 453, 462(sh), 471, 484(sh), 496, 506, 524(sh), 535 (sh), 552(sh)	2.82
$[Ir(df\text{-}ppy\text{-}CF_3)_2(ptb)]^+$	249, 266, 302(sh), 376, 405(sh)	470, 495	2.64	460, 493, 528(sh)	2.70

[a] Corrected for the change in instrument sensitivity across the wavelength range. The correction factor was established by using a light source with standard spectral irradiance. [b] 10 μM in acetonitrile. [c] 5 μM in 4:1 (v/v) ethanol/methanol.

Table 2. Selected computational data[16] and electrochemical properties.

	Calculated MO energies (BP86)		Reduction potential, $E^{0\prime}$ [V *vs* $Fc^{+/0}$][a]			Excited state potentials [V *vs* $Fc^{+/0}$][b][c]	
Complex	HOMO [eV]	LUMO [eV]	M^+/M	M/M^-	ΔE	M^+/M^*	M^*/M^-
$Ir(ppy)_3$	−4.622	−2.303	0.33	−2.67	3.00	−2.18	−0.16
$[Ru(bpy)_3]^{2+}$	−5.046	−3.278	0.89	−1.73, −1.92, −2.15	2.61	−1.24	0.40
$[Ir(df\text{-}ppy)_2(ptb)]^+$	−5.309	−2.818	1.18	−2.12	3.30	−1.59	0.65
$[Ir(df(CF_3)\text{-}ppy\text{-}Me)_2(ptb)]^+$	−5.498	−2.836	1.40 (1.37)[d]	−2.10 (−2.10)[d]	3.50 (3.47)[d]	−1.42	0.72
$[Ir(df(CN)\text{-}ppy)_2(ptb)]^+$	−5.654	−2.929	1.54 (1.53)[d]	−2.02[e] (−2.00)[d]	3.56 (3.53)[d]	−1.28	0.62
$[Ir(df\text{-}ppy\text{-}CF_3)_2(ptb)]^+$	−5.432	−3.013	1.35 (1.30)[d]	−1.88 (−1.92)[d]	3.23 (3.22)[d]	−1.35	0.82

[a] Cyclic voltammetry; electrodes: glassy carbon working, silver wire reference, platinum wire counter; 0.2 mM metal complex in dry acetonitrile with 0.1 M $TBAPF_6$; scan rate: 0.1 $V s^{-1}$. [b] Calculated from $E(M^+/M^*) = E(M^+/M) - E_{00} + w_r$ and $E(M^*/M^-) = E(M/M^-) + E_{00} + w_r$, where E_{00} is the difference between the zeroth vibrational energy levels of the ground and excited states, which can be estimated from the wavelength of maximum intensity in the low temperature photoluminescence emission spectra (Table 1), and w_r is a work term that can be assumed to be adequately included within the measurement of the ground-state potentials.[18] [c] The uncertainty in these estimates has been reported to be at least 100 mV.[18] [d] Predicted from the difference in MO energies compared to the $[Ir(df\text{-}ppy)_2(ptb)]^+$ complex. [e] E_p value for irreversible peak.

between those of the previously examined $[Ir(df\text{-}ppy)_2(ptb)]^+$ and $[Ir(df\text{-}ppy\text{-}CF_3)_2(ptb)]^+$, and the oxidation potential of $[Ir(df(CN)\text{-}ppy)_2(ptb)]^+$ (1.54 V *vs* $Fc^{+/0}$) is substantially higher than the other three Ir(III) complexes. The excited state potentials (Table 2) were calculated from the ground state potentials and the difference between the zeroth vibrational energy levels of the ground and excited states (E_{00}),[18] which was estimated from the wavelength of maximum intensity in the low temperature photoluminescence emission spectra (Table 1).

2.3 Annihilation ECL

The annihilation ECL spectra for the complexes are shown in Figure 2. The wavelengths of maximum intensity of $[Ir(df\text{-}ppy)_2(ptb)]^+$ (479 nm) $[Ir(df(CF_3)\text{-}ppy\text{-}Me)_2(ptb)]^+$ (472 nm) and $[Ir(df\text{-}ppy\text{-}CF_3)_2(ptb)]^+$ (490 nm) differ slightly from those of the photoluminescence (Table 1) due to the lower resolution of the CCD detector, but $[Ir(df(CN)\text{-}ppy)_2(ptb)]^+$ exhibited a large bathochromic shift from the blue photoluminescence to green ECL (530 nm). Moreover, the annihilation ECL intensity of this complex was very weak (Table 3). As shown in Table 2, the oxidation potential of this complex (1.54 V *vs* $Fc^{+/0}$) is higher than that of the other three complexes, towards the edge of the electrochemical window of the solvent. The change in emission color was therefore ascribed to degradation of the complex involving deleterious reactions with the radical intermediates of the concomitantly oxidized solvent.

The $[Ir(df\text{-}ppy\text{-}CF_3)_2(ptb)]^+$ complex exhibited the greatest annihilation ECL intensity (Figure 3d): 1.4-fold that of [Ir(df-

Table 3. Annihilation and co-reactant ECL intensities of the three $[Ir(df\text{-}ppy)_2(ptb)]^+$ derivatives relative to the parent complex.

	Annihilation ECL[a]	Co-reactant ECL with BPO[a]	Co-reactant ECL with TPrA[a]
$[Ir(df(CF_3)\text{-}ppy\text{-}Me)_2(ptb)]^+$	0.02	0.73	0.70
$[Ir(df(CN)\text{-}ppy)_2(ptb)]^+$	0.02[b]	0.10	0.01
$[Ir(df\text{-}ppy\text{-}CF_3)_2(ptb)]^+$	1.4	1.5	3.8

[a] Relative intensities were calculated by integrating the peak area of the ECL spectrum, then dividing by that obtained for $[Ir(df\text{-}ppy)_2(ptb)]^+$. Annihilation experiments were performed with a metal complex concentration of 0.2 mM in acetonitrile with 0.1 M $TBAPF_6$ as the electrolyte, using a glassy carbon, Pt wire and Ag/AgCl as the WE, CE and RE, respectively. The same conditions were used for the co-reactant ECL experiments with the addition of 5 mM BPO or 10 mM TPrA, and pulsing to 0.1 V beyond the relevant $E^{0\prime}$ of each complex. [b] A higher metal complex concentration of 0.4 mM and experiment time of 20 s was used to observe annihilation ECL from $[Ir(df(CN)\text{-}ppy)_2(ptb)]^+$.

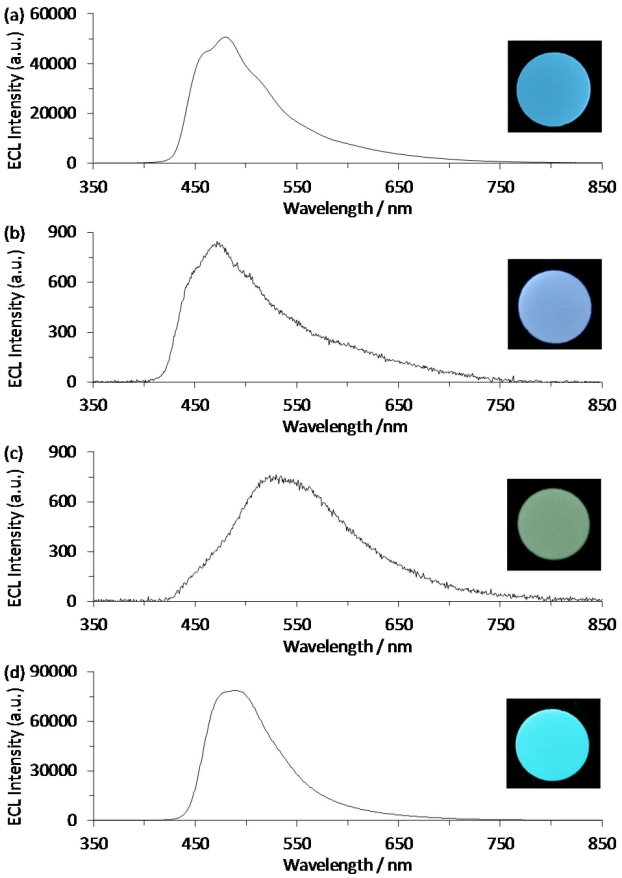

Figure 2. Annihilation ECL spectra and photographs of the emission at the working electrode for a) $[Ir(df\text{-}ppy)_2(ptb)]^+$, b) $[Ir(df(CF_3)\text{-}ppy\text{-}Me)_2(ptb)]^+$, c) $[Ir(df(CN)\text{-}ppy)_2(ptb)]^+$, and d) $[Ir(df\text{-}ppy\text{-}CF_3)_2(ptb)]^+$. Metal complexes were prepared at 0.2 mM and the first oxidation and reduction potentials (0.1 V past $E^{0\prime}$) were alternately applied at 20 Hz for 6 s, except for $[Ir(df(CN)\text{-}ppy)_2(ptb)]^+$, which was observed using a concentration of 0.4 mM and the 20 Hz pulse sequence was applied for 20 s.

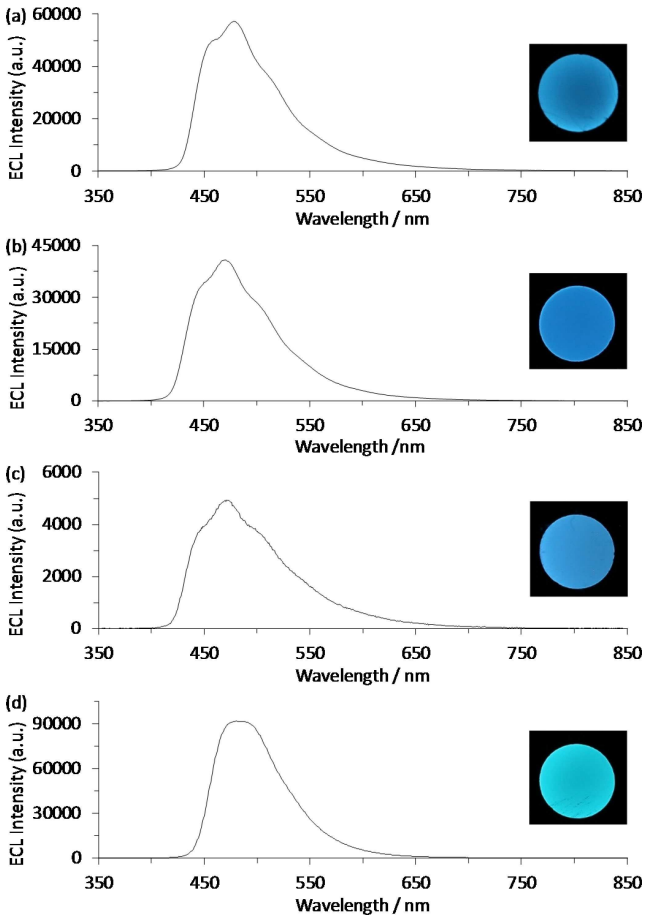

Figure 3. Cathodic co-reactant ECL spectra and photographs of the emission at the working electrode for a) $[Ir(df\text{-}ppy)_2(ptb)]^+$, b) $[Ir(df(CF_3)\text{-}ppy\text{-}Me)_2(ptb)]^+$, c) $[Ir(df(CN)\text{-}ppy)_2(ptb)]^+$, and d) $[Ir(df\text{-}ppy\text{-}CF_3)_2(ptb)]^+$, using 0.2 mM metal complex and 5 mM BPO. A potential of 0.1 V past $E^{0\prime}$ was applied at 20 Hz for 6 s.

$ppy)_2(ptb)]^+$ (Table 3) and over 4-fold that of $[Ru(bpy)_3]^{2+}$ (Table S1). The parent $[Ir(df\text{-}ppy)_2(ptb)]^+$ complex also showed (3-fold) greater annihilation ECL intensity than $[Ru(bpy)_3]^{2+}$.

2.4 Co-reactant ECL

We assessed the capabilities of the Ir(III) complexes as electrochemiluminophores for reductive-oxidation (cathodic) co-reactant ECL with BPO, as Swanick and co-workers had reported 4.5-fold greater ECL efficiency for $[Ir(df\text{-}ppy)_2(ptb)]^+$ than $[Ru(bpy)_3]^{2+}$ with this co-reactant.[6b] In contrast, we previously observed an ECL intensity of 6.2% for the $[Ir(df\text{-}ppy)_2(ptb)]^+$ complex relative to $[Ru(bpy)_3]^{2+}$ using oxidative-reduction (anodic) co-reactant ECL with TPrA.[17c] The BPO co-reactant is reduced at approximately −1.2 V *vs* $Fc^{+/0}$ (−0.8 V *vs* SCE[6a]) and generates a strong oxidant ($PhCO_2^{\bullet}$; Scheme 2). The potential of the $PhCO_2^{\bullet}/PhCO_2^-$ couple was estimated by Chandross and Sonntag[19] to be at least +1.1 V vs $Fc^{+/0}$ (+1.5 V *vs* SCE) but Akins and Birke[6a] later argued that +0.4 V *vs* $Fc^{+/0}$ (+0.8 V *vs* SCE) was more realistic. Based on the reduction potentials and low temperature emission energies of the complexes (Tables 1 and 2), an intermediate species with oxidation potential of between 0.65 V and 0.82 V (*vs* $Fc^{+/0}$) would be required to attain the excited state of these complexes via the pathway shown in Scheme 2. The potentials required to oxidize these complexes are between 1.18 and 1.54 V (*vs* $Fc^{+/0}$; Table 2), so alternative pathways[6b,8] involving their direct reaction with $PhCO_2^{\bullet}$ are unlikely.

As shown in Figure 3, we observed ECL from all four complexes when applying cathodic potentials (0.1 V beyond $E^{0\prime}$) with BPO as a co-reactant. The most effective electrochemiluminophore under these conditions was $[Ir(df\text{-}ppy\text{-}CF_3)_2(ptb)]^+$ with an intensity of 1.41 relative to $[Ir(df\text{-}ppy)_2(ptb)]^+$ (Table 3). The wavelengths of maximum ECL intensity were in good agreement with those of the corresponding photoluminescence (Table 1), with minor differences attributable to the lower resolution of the CCD spectrometer.

The absence of the large bathochromic shift in the cathodic co-reactant ECL for $[Ir(df(CN)\text{-}ppy)_2(ptb)]^+$ (Figure 3c) that was observed in its annihilation ECL (Figure 2c) supports the proposed degradation of the complex under oxidative poten-

tials. This was further validated by examining the relative anodic co-reactant ECL of the four complexes with TPrA (Table 3). Oxidation of this co-reactant ($E^{0\prime} \approx 0.5$ V *vs* $Fc^{+/0}$; 0.9 *vs* SCE) generates the α-amino radical $TPrA^{\bullet}$ (Scheme 1), which can reduce the oxidized metal complexes with sufficient energy to form the emitters. The reduction potentials of the four complexes are similar to the estimated potential of $TPrA^{\bullet}$, so it is possible that they are also reduced by this species. Subsequent reactions with $TPrA^{\bullet+}$ (a previously identified light-producing pathway in the $[Ru(bpy)_3]^{2+}$-TPrA system[4b]), however, are not sufficiently energetic to attain the excited states responsible for the emission.[4c]

The mechanism of anodic co-reactant ECL from these complexes with TPrA must therefore involve the oxidized metal complex, and under these conditions, the ECL intensity for the $[Ir(df(CN)\text{-}ppy)_2(ptb)]^+$ (relative to $[Ir(df\text{-}ppy)_2(ptb)]^+$) was an order of magnitude lower than that obtained in the cathodic co-reactant ECL with BPO.

2.5 Mixed Annihilation ECL with $Ir(ppy)_3$

Our previous work[16] demonstrated that the reaction between the electrochemically oxidized $[Ir(ppy)_3]^+$ and reduced $[Ir(df\text{-}ppy)_2(ptb)]^0$ ($E^{0\prime} = -2.12$ V *vs* $Fc^{+/0}$) species is sufficiently energetic to attain the $Ir(ppy)_3$* excited state, but the analogous reaction with the closely related $[Ir(df\text{-}ppy\text{-}CF_3)_2(ptb)]^0$ ($E^{0\prime} = -1.88$ V *vs* $Fc^{+/0}$) is insufficient. Calculations indicated that the SOMO energies of $[Ir(df(CF_3)\text{-}ppy\text{-}Me)_2(ptb)]^0$ and $[Ir(df(CN)\text{-}ppy)_2(ptb)]^0$ are between those of $[Ir(df\text{-}ppy)_2(ptb)]^0$ and $[Ir(df\text{-}ppy\text{-}CF_3)_2(ptb)]^0$ (Figure 4). As the SOMO energy of the $[Ir(df(CF_3)\text{-}ppy\text{-}Me)_2(ptb)]^0$ complex is greater than the LUMO energy of $[Ir(ppy)_3]^+$, the mixed annihilation ECL of $[Ir(df(CF_3)\text{-}ppy\text{-}Me)_2(ptb)]^+$ and $Ir(ppy)_3$ should also be energetically feasible. The SOMO energy of $[Ir(df(CN)\text{-}ppy)_2(ptb)]^0$ is also slightly higher than the LUMO energy of $[Ir(ppy)_3]^+$, but the values are too similar to confidently predict the outcome, based on the degree of error between relative MO energies and reduction potentials of a series of related complexes.[17c] The calculated reduction potential for $[Ir(df(CN)\text{-}ppy)_2(ptb)]^0$ of −2.02 *vs* $Fc^{+/0}$ (Table 2), however, is below the cut-off (−2.10 *vs* $Fc^{+/0}$) reported by Kapturkiewicz and Angulo[20] for the ECL reaction of organic nitriles/ketones with $Ir(ppy)_3$, whereas the reduction potential for $[Ir(df(CF_3)\text{-}ppy\text{-}Me)_2(ptb)]^0$ is at the cut-off value (Figure 5). We can, therefore, predict that efficient mixed annihilation ECL with $Ir(ppy)_3$ will be observed for $[Ir(df(CF_3)\text{-}ppy\text{-}Me)_2(ptb)]^+$ but not $[Ir(df(CN)\text{-}ppy)_2(ptb)]^0$.

To test if the $Ir(ppy)_3$* is attained upon reaction of the reduced $[Ir(C^{\wedge}N)_2(ptb)]^0$ complexes and $[Ir(ppy)_3]^+$, we applied potentials (0.1 V past $E^{0\prime}$) to generate these reactants and measured the resulting luminescence (or absence thereof) with a CCD spectrometer (Figure 6). As observed in our previous work, the reaction of $[Ir(df\text{-}ppy)_2(ptb)]^0$ and $[Ir(ppy)_3]^+$ resulted in intense green ECL from $Ir(ppy)_3$*, but the analogous reaction of $[Ir(df\text{-}ppy\text{-}CF_3)_2(ptb)]^0$ and $[Ir(ppy)_3]^+$ does not. The reaction of $[Ir(df(CF_3)\text{-}ppy\text{-}Me)_2(ptb)]^0$ and $[Ir(ppy)_3]^+$ also gave green ECL from $Ir(ppy)_3$* complex, at ~2-fold lower intensity than that of $[Ir(df\text{-}ppy)_2(ptb)]^0$ (Figure 6). We were unable to observe any emission from the reactions of $[Ir(df\text{-}ppy\text{-}CF_3)_2(ptb)]^0$ or $[Ir(df(CN)\text{-}ppy)_2(ptb)]^0$ and $Ir(ppy)_3{}^+$. The reductive-oxidation co-reactant ECL from these $[Ir(C^{\wedge}N)_2(ptb)]^+$ complexes with BPO (Figure 3) indicates that the reduced $[Ir(C^{\wedge}N)_2(ptb)]^0$ species are sufficiently stable to undergo subsequent electron transfer reactions, enabling the absence of mixed annihilation ECL to be confidently attributed to the energy required to attain $Ir(ppy)_3$*.

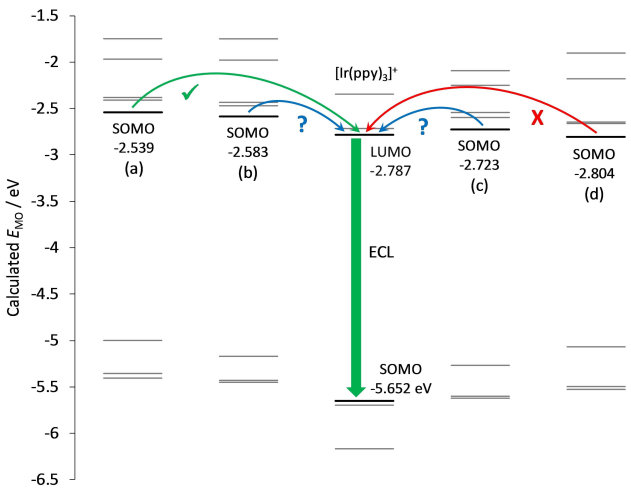

Figure 4. SOMO energies of a) $[Ir(df\text{-}ppy)_2(ptb)]^0$, b) $[Ir(df(CF_3)\text{-}ppy\text{-}Me)_2(ptb)]^0$, c) $[Ir(df(CN)\text{-}ppy)_2(ptb)]^0$, and d) $[Ir(df\text{-}ppy\text{-}CF_3)_2(ptb)]^0$ and the relevant MOs of $[Ir(ppy)_3]^+$. For $[Ir(C^{\wedge}N)_2(ptb)]^0$ complexes with SOMO energies above the LUMO of $[Ir(ppy)_3]^+$, the mixed annihilation ECL of $[Ir(C^{\wedge}N)_2(ptb)]^+$ and $Ir(ppy)_3$ is predicted to be energetically feasible.

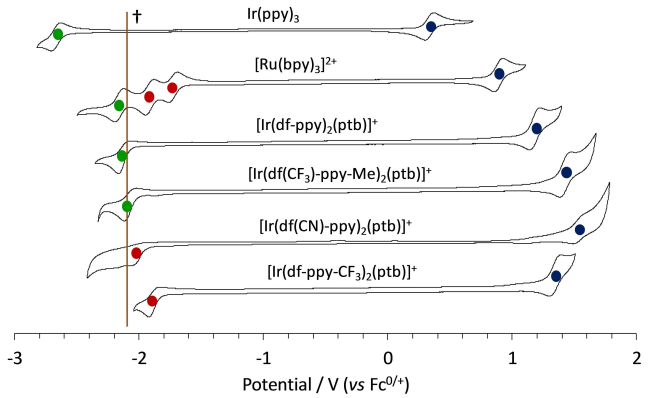

Figure 5. Cyclic voltammograms in dry acetonitrile at room temperature. The CVs were obtained at 0.2 mM with 0.1 M $TBAPF_6$ supporting electrolyte, at a scan rate of 0.1 $V\,s^{-1}$, using a glassy carbon working electrode, platinum wire counter electrode and silver wire reference electrode. Green dots = Reduction potentials of species capable of generating $Ir(ppy)_3$* upon reaction with $[Ir(ppy)_3]^+$. Red dots = Reduction potentials of species not capable of generating $Ir(ppy)_3$* upon reaction with $[Ir(ppy)_3]^+$. Blue dots = Potentials required to oxidize the complexes. †The cut-off potential reported by Kapturkiewicz and Angulo for organic nitriles/ketones to generate intense ECL with $[Ir(ppy)_3]^+$.[20]

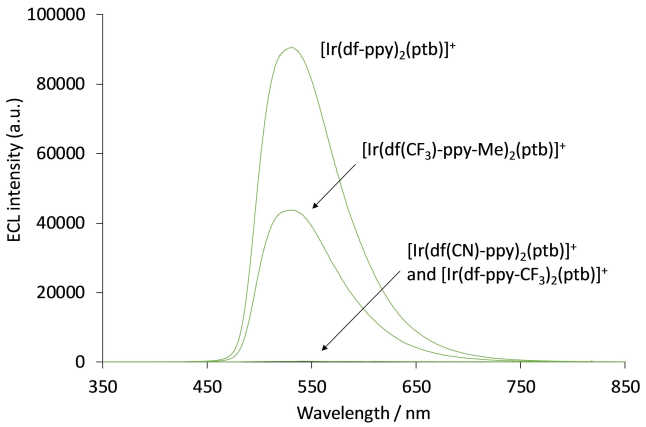

Figure 6. Mixed annihilation ECL between the $[Ir(C^{\wedge}N)_2(ptb)]^+$ complexes (0.2 mM) and $Ir(ppy)_3$ (0.01 mM) in acetonitrile with 0.1 M $TBAPF_6$ as the supporting electrolyte. The oxidation potential of $Ir(ppy)_3$ and the reduction potential of the $[Ir(C^{\wedge}N)_2(ptb)]^+$ complexes was applied (0.1 V past $E^{0\prime}$) at 10 Hz for 12 s. A 200 nm entrance slit was used in the CCD detector, which was coupled to the cell using an optical fiber and culminating lens, positioned below the working electrode. WE: glassy carbon; CE: Pt wire; RE: Ag wire.

3. Conclusion

Potentials for the oxidation and reduction of the three $[Ir(C^{\wedge}N)_2(ptb)]^+$ derivatives relative to the parent complex derived from DFT calculations were in good agreement (within 0.05 V) with experimentally determined values, and enabled accurate prediction of the energy sufficiency of a mixed annihilation ECL system. Although the $[Ir(df\text{-}ppy\text{-}CF_3)_2(ptb)]^+$ complex does not exhibit efficient mixed annihilation ECL with $Ir(ppy)_3$, it generated the most intense conventional annihilation ECL, oxidative-reduction co-reactant ECL with TPrA, and reductive-oxidation co-reactant ECL with BPO, of the four blue luminophores, demonstrating its great potential for a broad range of applications.

Experimental Section

Chemicals

fac-Tris(2-phenylpyridine)iridium(III) ($Ir(ppy)_3$) was purchased from Rubipy Scientific (Canada). Bis[3,5-difluoro-2-(2-pyridinyl-κ**N**)phenyl-κ**C**][2-[1-(phenylmethyl)-1**H**-1,2,3-triazol-4-yl-κ**N**^{3}]pyridine-κ**N**]iridium(1+) hexafluorophosphate(1-) (**[Ir(df-ppy)$_2$(ptb)](PF$_6$)**) and bis[3,5-difluoro-2-(5-(trifluoromethyl)-2-pyridinyl-κ**N**)phenyl-κ**C**][2-[1-(phenylmethyl)-1**H**-1,2,3-triazol-4-yl-κ**N**^{3}]pyridine-κ**N**]iridium(1+) hexafluorophosphate(1-) (**[Ir(df-ppy-CF$_3$))$_2$(ptb)](PF$_6$)**) were synthesized and characterized in our previous studies.[16,17c,21] The Ir(III) dimers: di-μ-chlorotetrakis[4-cyano-3,5-difluoro-2-(2-pyridinyl-κN)phenyl-κC]diiridium ($[Ir(df(CN)\text{-}ppy)_2(\mu\text{-}Cl)]_2$) and di-μ-chlorotetrakis[3,5-difluoro-2-(4-methyl-2-pyridinyl-κN)-4-(trifluoromethyl)phenyl-κC]diiridium ($[Ir(df(CF_3)\text{-}ppy\text{-}Me)_2(\mu\text{-}Cl)]_2$) were from Luminescence Technology Corp. (Taiwan). Ferrocene was obtained from Strem Chemicals (USA). Potassium chloride for reference electrode storage was purchased from Labserv Pronalys (Australia). Acetonitrile (Scharlau, Spain) was distilled over calcium hydride under a nitrogen atmosphere. Benzoyl peroxide (BPO) was purchased from Fluka Analytical (Switzerland) and was directly dissolved into the solvent prior to experimentation.

NMR spectra were acquired on a Bruker Biospin AV400 spectrometer. $^{13}C\{^1H\}$ NMR spectra were acquired at 100 MHz, ^1H NMR spectra were acquired at 400 MHz, and ^{19}F NMR acquired at 376 MHz. All NMR spectra were recorded at 298 K. Chemical shifts were referenced to residual solvent peaks and are quoted in terms of parts per million (ppm), relative to tetramethylsilane ($Si(CH_3)_4$); ^{19}F NMR signals are quoted relative to an internal standard of hexafluorobenzene. Electrospray ionization mass spectra (ESI-MS) were acquired using an Exactive Plus Orbitrap Mass Spectrometer (Thermo Scientific).

[Ir(df(CF$_3$)-ppy-Me)$_2$(ptb)](PF$_6$)

The dimer $[Ir(df(CF_3)\text{-}ppy\text{-}Me)_2(\mu\text{-}Cl)]_2$ (150 mg, 97 μmol) and 2-(1-(benzyl)-1*H*-1,2,3-triazol-4-yl)pyridine (ptb, 46 mg, 194 μmol) were suspended in a 3:1 mixture of dichloromethane and methanol. Starting materials typically solubilized within 1 h. Reactions were stirred in darkness under an inert atmosphere for 16 h. The solvents were then removed, and the residue dissolved in acetonitrile and filtered through a filter aid (Celite). The solvent was then removed by evaporation under reduced pressure and the residue re-dissolved in a minimum amount of ethanol and filtered through filter aid (Celite). To this solution was added a saturated aqueous solution of ammonium hexafluorophosphate until precipitation of a brightly colored solid began to occur. The mixture was stirred in darkness for 16 h, and the product was then collected by filtration and washed with water, cold ethanol, ether, and lastly pentane, and then dried *in vacuo* to yield the product as a pale-yellow solid (190 mg, 87%). ^1H NMR (400 MHz; CD_2Cl_2): δ 8.69 (1H, s, ptb-triazolyl-*H*), 8.16–8.21 (3H, m, pyridyl-*H*, ptb-pyridyl-*H*), 8.08 (1H, td, J = 7.9, 1.6 Hz, ptb-pyridyl-*H*), 7.83 (1H, d, J = 5.4 Hz, ptb-pyridyl-*H*), 7.46 (1H, d, J = 6.0 Hz, pyridyl-*H*), 7.30–7.43 (7H, m, pyridyl-*H*, ptb-pyridyl-*H*, ptb-phenyl-*H*), 7.00 (1H, d, J = 6.0 Hz, pyridyl-*H*), 6.93 (1H, d, J = 6.0 Hz, pyridyl-*H*), 5.94 (1H, d, J = 10.7 Hz, phenyl-*H*), 5.89 (1H, d, J = 10.8 Hz, phenyl-*H*), 5.61 (2H, s, ptb-triazole-CH_2-phenyl), 2.56 (3H, s, pyridyl-CH_3), 2.55 (3H, s, pyridyl-CH_3). ^{19}F NMR (376 MHz; CD_2Cl_2): δ −57.9 (t, J = 23.1 Hz), −58.0 (t, J = 23.1 Hz), −74.7 (d, J = 711.4 Hz), −111.6 (qd, J = 23.2, 5.2 Hz), −112.6 (qd, J = 23.2, 5.0 Hz), −114.5 (qd, J = 23.0, 5.2 Hz), −115.6 (qd, J = 23.0, 4.9 Hz). $^{13}C\{^1H\}$ NMR was not obtained as peak splitting due to multiple fluorine nuclei in the molecule prevented clear resolution of all peaks. ESI-MS: Calculated for $C_{40}H_{26}F_{10}IrN_6^+$ ($[M]^+$): *m/z* 973.168. Found *m/z* 973.1708.

[Ir(df(CN)-ppy)$_2$(ptb)](PF$_6$)

The dimer $[Ir(df(CN)\text{-}ppy)_2(\mu\text{-}Cl)]_2$ (150 mg, 114 μmol) and 2-(1-(benzyl)-1*H*-1,2,3-triazol-4-yl)pyridine (54 mg, 228 μmol) were suspended in a 3:1 mixture of dichloromethane and methanol. Starting materials typically solubilized within 1 h. Reactions were stirred in darkness under an inert atmosphere for 16 h. The solvents were then removed and the residue dissolved in acetonitrile and filtered through a filter aid (Celite). The solvent was then removed by evaporation under reduced pressure and the residue re-dissolved in a minimum amount of acetonitrile and filtered through filter aid (Celite). To this solution was added a saturated aqueous solution of ammonium hexafluorophosphate until precipitation of a brightly colored solid began to occur. The mixture was stirred in darkness for 16 h, and the crude product was then collected by filtration and washed with diethyl ether. The crude product was then re-crystallized from a mixture of acetonitrile and diethyl ether to give the product as a pale-yellow solid (99 mg, 43%). (400 MHz; CD_3CN): δ 8.60 (1H, s, ptb-triazolyl-*H*), 8.36 (2H, t, J = 8.0 Hz, pyridyl-

H), 8.11 (2H, m, ptb-pyridyl-*H*), 8.02 (2H, t, J = 7.96, pyridyl-*H*), 7.83 (1H, d, J = 5.6 Hz, ptb-pyridyl-*H*), 7.76 (1H, d, J = 6.0 Hz, phenyl-*H*), 7.63 (1H, d, J = 5.8 Hz, phenyl-*H*), 7.37–7.44 (4H, m, ptb-phenyl-*H*, ptb-pyridyl-*H*), 7.22–7.27 (3H, m, ptb-phenyl-*H*, pyridyl-*H*), 7.19 (1H, ddd, J = 7.4, 5.9, 1.4 Hz, pyridyl-*H*), 6.03 (1H, d, J = 8.7 Hz, phenyl-*H*), 5.98 (1H, d, J = 8.9 Hz, phenyl-*H*), 5.58 (2H, m, ptb-triazole-CH_2-phenyl). $^{13}C\{^1H\}$ NMR (100 MHz; CD_3CN): δ 56.7, 87.6, 111.2, 111.3, 116.0 (t, J = 3.2 Hz), 116.2 (t, J = 3.2 Hz), 124.4, 125.1, 125.3, 125.4, 125.6, 126.2, 126.4, 127.5, 128.3, 129.5 (2 C), 130.1 (2 C), 130.2, 130.5 (dd, J = 15.3, 3.1 Hz), 130.6 (dd, J = 15.3, 2.5 Hz), 134.1, 141.3 (2 C), 141.8, 149.5, 149.6, 151.0, 151.3, 151.9, 160.3 (dd, J = 220.9, 4.7 Hz), 160.6 (d, J = 7.3 Hz), 161.0 (dd, J = 220.9, 4.8 Hz), 162.6 (d, J = 7.2 Hz), 162.9 (d, J = 7.0 Hz), 163.0 (dd, J = 211.8, 4.4 Hz), 163.2 (d, J = 7.5 Hz), 163.5 (dd, J = 240.0, 3.2 Hz). ^{19}F NMR (376 MHz; CD_3CN): δ −73.4 (d, J = 706.3 Hz), −106.0 (d, J = 3.9 Hz), −106.8 (d, J = 3.5 Hz), −107.4 (d, J = 3.9 Hz), −108.3 (d, J = 3.5 Hz). ESI-MS: Calculated for $C_{38}H_{22}F_4IrN_8^+$ ($[M]^+$): *m/z* 859.153. Found *m/z* 859.1534.

Absorption and Photoluminescence Emission

Spectra were collected using a Cary 300 Bio UV/Vis spectrophotometer (Varian Australia, Australia) and a Cary Eclipse fluorescence spectrophotometer (5 nm band pass, 1 nm data interval, PMT voltage: 800 V; Varian Australia), with Spectrosil Quartz fluorimeter cuvettes (Starna, Australia). Low temperature photoluminescence spectra were obtained using an OptistatDN Variable Temperature Liquid Nitrogen Cryostat (Oxford Instruments, U.K.), with custom-made quartz sample holder.[16] Emission spectra were corrected for the change in instrument sensitivity across the wavelength range.[22] The low temperature spectra were collected at 85 K to avoid damage to the spectroscopic cuvettes.[23] We previously found no significant difference in λ_{max} in the spectra of $[Ru(bpy)_3]^{2+}$ and Ir$(ppy)_3$ measured at 85 K and 77 K under these instrumental conditions.[16]

Electrochemistry and ECL

The electrochemical setup consisted of a glass electrochemical cell with a flat base and Teflon lid[10c] that was custom made to fit the electrodes and gas line. A glassy carbon working electrode, platinum wire counter electrode (CH Instruments, USA) and either an Ag wire or Ag/AgCl leak free reference electrode (eDAQ, Australia) were used for all experiments. The cell was held in a light-tight faraday cage. Electrochemical experiments were controlled with an Autolab PGSTAT204 or PGSTAT128 N potentiostat (Metrohm Autolab B.V., Netherlands). An internal reference, the ferrocenium/ferrocene ($Fc^{+/0}$) couple (0.2 mM), was used in situ to reference all oxidation and reduction potentials. An Ocean Optics collimating lens (Ocean Optics 74-UV, 200–2000 nm) was positioned directly under the working electrode and coupled with an optical fiber (1.0 m length, 1.0 mm core diameter) and an Ocean Optics QEpro CCD spectrometer, which was used to collect ECL emission spectra. Images of the ECL were taken with a Canon EOS 6D DSLR camera (Canon, Japan) fitted with a Tonika AT-X PRO MACRO 100 mm f/2.8 D lens (Kenko Tonika Co., Japan) which was manually focused on the surface of the working electrode, and remotely controlled by the potentiostat.[12] Acetonitrile was used as the solvent with 0.1 M $TBAPF_6$ as the supporting electrolyte. The working electrode was polished using 0.3 mm and 0.05 mm alumina powder on a felt pad. All of the electrodes were cleaned using acetone and then dried with nitrogen or argon gas.

Computational Methods

DFT calculations were carried out within the Gaussian 16 suite of programs.[24] Ground state singlet and triplet geometries were optimized in the presence of solvent with the BP86 functional[25] in conjunction with the def2-TZVP basis set and associated core potential.[26] For Ir$(ppy)_3$, the mPW1PW91 functional[27] was used as geometry optimization with BP86 proved problematic. The polarizable continuum model (PCM)[28] self-consistent reaction field (SCRF) was used to model solvent effects with Truhlar's SMD solvent model,[29] with a solvent of acetonitrile for consistency with the experimental system. Stationary points were characterized as minima by calculating the Hessian matrix analytically at the same level of theory. All structures are minima with no imaginary frequencies. Molecular orbitals were calculated at the BP86/def2-TZVP level of theory, which has previously been demonstrated to produce reliable results.[17c,30] Molecular orbital analysis was carried out with the QMForge program.[31]

Acknowledgements

This work was funded by the Australian Research Council (DP160103046; DP180100094) and the Office of Naval Research Global (N62909-18-1-2024). LCS is supported by a Deakin University Postgraduate Scholarship. We acknowledge generous allocations of computing from La Trobe University, Intersect, and NCI.

Keywords: Electrochemiluminescence · electrogenerated chemiluminescence · electrochemically initiated luminescence · density functional theory · iridium complexes

[1] a) N. Sojic, S. Arbault, L. Bouffier, A. Kuhn, *in Luminescence* (Eds.: F. Misomandre, P. Audebert), Springer, Gewerbestrasse, Switzerland, **2017**, pp. 257–291; b) L. Li, Y. Chen, J.-J. Zhu, *Anal. Chem.* **2017**, *89*, 358–371; c) E. H. Doeven, G. J. Barbante, C. F. Hogan, P. S. Francis, *ChemPlusChem* **2015**, *80*, 456–470; d) Z. Liu, W. Qi, G. Xu, *Chem. Soc. Rev.* **2015**, *44*, 3117–3142.

[2] W. Miao, *Chem. Rev.* **2008**, *108*, 2506–2553.

[3] M.-M. Chang, T. Saji, A. J. Bard, *J. Am. Chem. Soc.* **1977**, *99*, 5399–5403.

[4] a) J. K. Leland, M. J. Powell, *J. Electrochem. Soc.* **1990**, *137*, 3127–3131; b) W. Miao, J.-P. Choi, A. J. Bard, *J. Am. Chem. Soc.* **2002**, *124*, 14478–14485; c) E. Kerr, E. H. Doeven, D. J. D. Wilson, C. F. Hogan, P. S. Francis, *Analyst* **2016**, *141*, 62–69.

[5] a) C. M. Hindson, P. S. Francis, G. R. Hanson, N. W. Barnett, *Chem. Commun.* **2011**, *47*, 7806–7808; b) T. Kai, M. Zhou, S. Johnson, H. S. Ahn, A. J. Bard, *J. Am. Chem. Soc.* **2018**, *140*, 16178–16183; c) H. C. Moon, T. P. Lodge, C. D. Frisbie, *Chem. Mater.* **2014**, *26*, 5358–5364.

[6] a) D. L. Akins, R. L. Birke, *Chem. Phys. Lett.* **1974**, *29*, 428–435; b) K. N. Swanick, S. Ladouceur, E. Zysman-Colman, Z. Ding, *Chem. Commun.* **2012**, *48*, 3179–3181; c) S. Kesarkar, E. Rampazzo, G. Valenti, M. Marcaccio, A. Bossi, L. Prodi, F. Paolucci, *ChemElectroChem* **2017**, *4*, 1690–1696; d) C.-W. Hsu, E. Longhi, S. Sinn, C. S. Hawes, D. C. Young, P. E. Kruger, L. De Cola, *Chem. Asian J.* **2017**, *12*, 1649–1658.

[7] a) H. S. White, A. J. Bard, *J. Am. Chem. Soc.* **1982**, *104*, 6891–6895; b) F. Bolletta, M. Ciano, V. Balzani, N. Serpone, *Inorg. Chim. Acta* **1982**, *62*, 207–213.

[8] J. Rosenthal, A. B. Nepomnyashchii, J. Kozhukh, A. J. Bard, S. J. Lippard, *J. Phys. Chem. C* **2011**, *115*, 17993–18001.

[9] A. Kapturkiewicz, *Anal. Bioanal. Chem.* **2016**, *408*, 7013–7033.

[10] a) H. C. Moon, T. P. Lodge, C. D. Frisbie, *J. Am. Chem. Soc.* **2014**, *136*, 3705–3712; b) K. N. Swanick, M. Sandroni, Z. Ding, E. Zysman-Colman, *Chem. Eur. J.* **2015**, *21*, 7435–7440; c) E. Kerr, E. H. Doeven, G. J. Barbante, C. F. Hogan, D. J. Hayne, P. S. Donnelly, P. S. Francis, *Chem. Sci.* **2016**, *7*,

5271–5279; d) L. C. Soulsby, E. H. Doeven, T. T. Pham, D. J. Eyckens, L. C. Henderson, B. M. Long, R. M. Guijt, P. S. Francis, *Chem. Commun.* **2019**, *55*, 11474–11477; e) H. Oh, D. G. Seo, H. C. Moon, *Org. Electron.* **2018**, *65*, 394–400.

[11] E. Kerr, E. H. Doeven, G. J. Barbante, C. F. Hogan, D. Bower, P. S. Donnelly, T. U. Connell, P. S. Francis, *Chem. Sci.* **2015**, *6*, 472–479.

[12] L. C. Soulsby, D. J. Hayne, E. H. Doeven, L. Chen, C. F. Hogan, E. Kerr, J. L. Adcock, P. S. Francis, *ChemElectroChem* **2018**, *5*, 1543–1547.

[13] a) D. Bruce, M. M. Richter, *Anal. Chem.* **2002**, *74*, 1340–1342; b) E. H. Doeven, E. M. Zammit, G. J. Barbante, C. F. Hogan, N. W. Barnett, P. S. Francis, *Angew. Chem. Int. Ed.* **2012**, *51*, 4354–4357; *Angew. Chem.* **2012**, *124*, 4430–4433; c) E. H. Doeven, E. M. Zammit, G. J. Barbante, P. S. Francis, N. W. Barnett, C. F. Hogan, *Chem. Sci.* **2013**, *4*, 977–982; d) E. H. Doeven, G. J. Barbante, E. Kerr, C. F. Hogan, J. A. Endler, P. S. Francis, *Anal. Chem.* **2014**, *86*, 2727–2732; e) G. J. Barbante, N. Kebede, C. M. Hindson, E. H. Doeven, E. M. Zammit, G. R. Hanson, C. F. Hogan, P. S. Francis, *Chem. Eur. J.* **2014**, *20*, 14026–14031; f) Y.-Z. Wang, C.-H. Xu, W. Zhao, Q.-Y. Guan, H.-Y. Chen, J.-J. Xu, *Anal. Chem.* **2017**, *89*, 8050–8056; g) M. R. Moghaddam, S. Carrara, C. F. Hogan, *Chem. Commun.* **2019**, *55*, 1024–1027.

[14] a) S. Laird, C. F. Hogan, *in Iridium(III) in Optoelectronic and Photonics Applications* (Ed.: E. Zysman-Colman), John Wiley & Sons, Inc., Chichester, UK, **2017**, pp. 359–414; b) M. A. Haghighatbin, S. E. Laird, C. F. Hogan, *Curr. Opin. Electrochem.* **2018**, *8*, 52–59; c) L. Chen, D. J. Hayne, E. H. Doeven, J. Agugiaro, D. J. D. Wilson, L. C. Henderson, T. U. Connell, Y. H. Nai, R. Alexander, S. Carrara, C. F. Hogan, P. S. Donnelly, P. S. Francis, *Chem. Sci.* **2019**, *10*, 8654–8667.

[15] a) S. Zhu, Q. Song, S. Zhang, Y. Ding, *J. Mol. Struct.* **2013**, *1035*, 224–230; b) J. M. Younker, K. D. Dobbs, *J. Phys. Chem. C* **2013**, *117*, 25714–25723; c) T. B. Demissie, K. Ruud, J. H. Hansen, *Organometallics* **2015**, *34*, 4218–4228.

[16] L. C. Soulsby, D. J. Hayne, E. H. Doeven, D. J. D. Wilson, J. Agugiaro, T. U. Connell, L. Chen, C. F. Hogan, E. Kerr, J. L. Adcock, P. S. Donnelly, J. M. White, P. S. Francis, *Phys. Chem. Chem. Phys.* **2018**, *20*, 18995–19006.

[17] a) M. Mydlak, C. Bizzarri, D. Hartmann, W. Sarfert, G. Schmid, L. De Cola, *Adv. Funct. Mater.* **2010**, *20*, 1812–1820; b) S. Zanarini, M. Felici, G. Valenti, M. Marcaccio, L. Prodi, S. Bonacchi, P. Contreras-Carballada, R. M. Williams, M. C. Feiters, R. J. M. Nolte, L. De Cola, F. Paolucci, *Chem. Eur. J.* **2011**, *17*, 4640–4647; c) G. J. Barbante, E. H. Doeven, E. Kerr, T. U. Connell, P. S. Donnelly, J. M. White, T. Lópes, S. Laird, C. F. Hogan, D. J. D. Wilson, P. J. Barnard, P. S. Francis, *Chem. Eur. J.* **2014**, *20*, 3322–3332.

[18] W. E. Jones Jr., M. A. Fox, *J. Phys. Chem.* **1994**, *98*, 5095–5099.

[19] E. A. Chandross, F. I. Sonntag, *J. Am. Chem. Soc.* **1966**, *88*, 1089–1096.

[20] A. Kapturkiewicz, G. Angulo, *Dalton Trans.* **2003**, 3907–3913.

[21] T. U. Connell, J. M. White, T. A. Smith, P. S. Donnelly, *Inorg. Chem.* **2016**, *55*, 2776–2790.

[22] P. S. Francis, J. L. Adcock, N. W. Barnett, *Spectrochim. Acta Part A* **2006**, *65*, 708–710.

[23] C. Mallet, A. Bolduc, S. Bishop, Y. Gautier, W. G. Skene, *Phys. Chem. Chem. Phys.* **2014**, *16*, 24382–24390.

[24] M. J. Frisch, G. W. Trucks, H. B. Schlegel, G. E. Scuseria, M. A. Robb, J. R. Cheeseman, G. Scalmani, V. Barone, G. A. Petersson, H. Nakatsuji, X. Li, M. Caricato, A. V. Marenich, J. Bloino, B. G. Janesko, R. Gomperts, B. Mennucci, H. P. Hratchian, J. V. Ortiz, A. F. Izmaylov, J. L. Sonnenberg, D. Williams-Young, F. Ding, F. Lipparini, F. Egidi, J. Goings, B. Peng, A. Petrone, T. Henderson, D. Ranasinghe, V. G. Zakrzewski, J. Gao, N. Rega, G. Zheng, W. Liang, M. Hada, M. Ehara, K. Toyota, R. Fukuda, J. Hasegawa, M. Ishida, T. Nakajima, Y. Honda, O. Kitao, H. Nakai, T. Vreven, K. Throssell, J. A. Montgomery, Jr., J. E. Peralta, F. Ogliaro, M. J. Bearpark, J. J. Heyd, E. N. Brothers, K. N. Kudin, V. N. Staroverov, T. A. Keith, R. Kobayashi, J. Normand, K. Raghavachari, A. P. Rendell, J. C. Burant, S. S. Iyengar, J. Tomasi, M. Cossi, J. M. Millam, M. Klene, C. Adamo, R. Cammi, J. W. Ochterski, R. L. Martin, K. Morokuma, O. Farkas, J. B. Foresman, D. J. Fox, Gaussian, Inc., Wallingford CT, **2016**.

[25] a) A. D. Becke, *Phys. Rev. A: Gen. Phys.* **1988**, *38*, 3098–3100; b) J. P. Perdew, *Phys. Rev. B* **1986**, *33*, 8822–8824.

[26] F. Weigend, R. Ahlrichs, *Phys. Chem. Chem. Phys.* **2005**, *7*, 3297–3305.

[27] C. Adamo, V. Barone, *J. Chem. Phys.* **1998**, *108*, 664–675.

[28] J. Tomasi, B. Mennucci, R. Cammi, *Chem. Rev.* **2005**, *105*, 2999–3093.

[29] A. V. Marenich, C. J. Cramer, D. G. Truhlar, *J. Phys. Chem. B* **2009**, *113*, 6378–6396.

[30] L. Chen, E. H. Doeven, D. J. D. Wilson, E. Kerr, D. J. Hayne, C. F. Hogan, W. Yang, T. T. Pham, P. S. Francis, *ChemElectroChem* **2017**, *4*, 1797–1808.

[31] A. L. Tenderholt. QMForge, Version 2.4, https://qmforge.net/.

Manuscript received: January 1, 2020
Revised manuscript received: February 5, 2020

ARTICLES

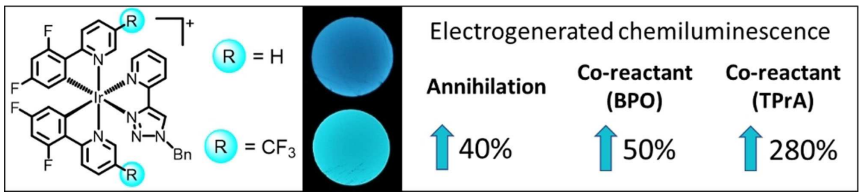

Feeling blue: The influence of electron-withdrawing/donating substituents on the electrogenerated chemiluminescence (ECL) of a benchmark blue luminophore $[Ir(df\text{-}ppy)_2(ptb)]^+$ (where df-ppy = 2-(2,4-difluorophenyl)-pyridine anion; ptb = 1-benzyl-1,2,3-triazol-4-ylpyridine) is explored, providing new insight into the ECL of iridium complexes, and revealing a trifluoromethyl derivative as a superior blue electrochemiluminophore.